Abbreviated Terms

The following abbreviations are used throughout this chapter:

Abbreviation	**Full Term**
Characteristic Functions	
V	Point characteristic (position $\to$ position)
T	Angle characteristic (direction $\to$ direction)
W	Mixed characteristic (position $\to$ direction)
W'	Mixed characteristic (direction $\to$ position)
Optical Terms	
OPL	Optical Path Length
OPD	Optical Path Difference
WFE	Wavefront Error
RMS	Root Mean Square
P-V	Peak-to-Valley
PSF	Point Spread Function
MTF	Modulation Transfer Function
NA	Numerical Aperture
Aberration Terms	
S_I – S_V	Seidel aberration coefficients
W_{040}	Spherical aberration coefficient
W_{131}	Coma coefficient
W_{222}	Astigmatism coefficient
Computational Terms	
DEE	Differentiable Eikonal Engine
JAX	Google's autodiff library
WKB	Wentzel-Kramers-Brillouin approximation

Chapter 2
Hamilton's Characteristic Functions

Learning Objectives

After completing this chapter, you will be able to:

1. Master Hamilton's four characteristic functions (V, T, W, W') and their physical interpretations
2. Select the appropriate characteristic function for each optical conjugate configuration
3. Derive ray mapping equations and Seidel aberrations from characteristic function expansions
4. Apply the Legendre transform relationships connecting all four functions
5. Implement differentiable characteristic function computation using JAX
6. Apply the Walther-Matsui/Nariai duality for analysis and design
7. Connect characteristic functions to quantum propagators via the Hamilton-Jacobi equation

2.1 Chapter Pain Points

Hamilton's characteristic functions can feel abstract on first contact, so we start with the three recurring engineering uses that motivate this chapter. In day-to-day work, we either analyze a known lens prescription (forward), synthesize a lens to hit a target aberration profile (inverse), or reinterpret the same scalar quantity as a phase object that also governs quantum propagation. The three boxes below state these use-cases in their most practical form. Read each box as: (i) the question you actually ask, (ii) the situation that triggers it, and (iii) how DEE turns it into a systematic computation.

WALTHER Pain Point (Forward Analysis)

"I have a lens system with known surfaces. How do I systematically compute the characteristic functions that completely describe its imaging behavior at any field angle?"
Situation: You have a complete lens prescription. You need to extract the fundamental optical properties that govern image formation.
DEE Solution: Hamilton's characteristic functions provide a systematic framework to compute all imaging properties from surface data.

MATSUI-NARIAI Pain Point (Inverse Design)

"I need specific imaging properties—corrected coma, flat field, minimal distortion. What combination of surface curvatures and spacings will achieve my target characteristic function?"
Situation: Your specification demands particular aberration behavior. Traditional optimization struggles with the many-parameter design space.
DEE Solution: The Matsui-Nariai framework inverts the characteristic function computation, using JAX autodiff to find parameters achieving target specifications.

QUANTUM EXTENSION

Quantum Extension: "How does the classical characteristic function become the quantum propagator, and what does this mean for photonic device design?"
The bridge identity $\phi_{\text{quantum}} = 2\pi W/\lambda$ establishes mathematical equivalence between classical aberrations and quantum phase errors.

Throughout the chapter, we will repeatedly return to these three questions—first deriving the four characteristic functions and their relations, then showing how DEE makes them differentiable, and finally using the same bridge to connect classical aberrations to quantum phase errors.

2.2 Introduction: Why Characteristic Functions?

Every optical system transforms light from object space to image space. Hamilton's profound insight was that this transformation can be completely characterized by a single scalar function—the optical path length between conjugate points [1]. This reduction from vector ray tracing to scalar function manipulation is the foundation of modern aberration theory.

Key Insight

Hamilton's characteristic functions encode the complete imaging properties of any optical system in a single scalar function. All aberrations, ray mappings, and wavefront deformations can be extracted by differentiation.

The power of this approach becomes evident when we consider computational implications:

- **Ray tracing:** Trace each ray individually through every surface ($O(N_{\text{rays}} \times N_{\text{surfaces}})$)
- **Characteristic functions:** Evaluate a polynomial expansion ($O(N_{\text{coeffs}})$)

For systems with many surfaces or requiring dense ray sampling, the characteristic function approach can provide orders-of-magnitude speedup while maintaining full physical accuracy within the eikonal approximation.

This chapter develops Hamilton's systematic framework of characteristic functions, then extends it to modern differentiable computing and quantum photonics—establishing the theoretical bridges that unify classical lens design with emerging computational and quantum applications.

2.3 Hamilton's Four Characteristic Functions

Hamilton identified four characteristic functions, distinguished by whether object and image points are specified by position or direction [3, 4]. Each function serves a particular conjugate configuration, and all are related by Legendre transforms.

2.3.1 The Point Characteristic $V(\mathbf{r}, \mathbf{r}')$

Introduction: The point characteristic V gives the optical path length between two spatial points, forming the foundation of Hamilton's theory. William Rowan Hamilton, in his seminal 1828 paper "Theory of Systems of Rays" [1], recognized that any optical system can be completely characterized by this single scalar function.

Definition:

$$V(\mathbf{r}, \mathbf{r}') = \int_{\mathbf{r}}^{\mathbf{r}'} n \, ds \tag{2.1}$$

where the integral is taken along the ray connecting $\mathbf{r}$ and $\mathbf{r}'$.

Development: The gradients yield the ray directions:

$$\nabla_{\mathbf{r}} V = -n\hat{\mathbf{s}} \quad \text{(outgoing from object)} \tag{2.2}$$

$$\nabla_{\mathbf{r}'} V = n'\hat{\mathbf{s}}' \quad \text{(incoming to image)} \tag{2.3}$$

Physical Interpretation: V answers the question "how much optical phase accumulates when light travels from object point P to image point P'?" This is precisely the information needed for diffraction calculations and quantum phase analysis.

Turn—DEE Implementation:

Table 2.1: Point Characteristic V—Classical, DEE, and Quantum Perspectives

Aspect	**Classical**	**DEE Implementation**	**Quantum Analog**
Core quantity	OPL: $V = \int n \, ds$	`V = jnp.sum(n*segments)`	Propagator phase
Gradient	Ray direction: $\nabla V/n$	`jax.grad(V)`	Momentum operator
Physical meaning	Path length	Differentiable integral	Feynman kernel $K(\mathbf{r}', \mathbf{r})$

Conclusion: The point characteristic is most useful for microscope objectives and relay systems where both object and image are at finite distances.

2.3.2 The Angle Characteristic $T(\mathbf{p}, \mathbf{p}')$

Introduction: The angle characteristic T uses direction cosines instead of positions, making it ideal for afocal systems where both object and image are at infinity.

Definition via Legendre Transform:

$$T(\mathbf{p}, \mathbf{p}') = V + \mathbf{r} \cdot \mathbf{p} - \mathbf{r}' \cdot \mathbf{p}' \tag{2.4}$$

where $\mathbf{p} = n(L, M, N)$ is the optical direction vector.

Development: The gradients now give spatial coordinates:

$$\nabla_{\mathbf{p}} T = \mathbf{r} \quad \text{(object position)} \tag{2.5}$$

$$\nabla_{\mathbf{p}'} T = -\mathbf{r}' \quad \text{(image position)} \tag{2.6}$$

Turn—Applications: T is the natural choice for:

- Telescopes (object at infinity, image at infinity in afocal mode)
- Beam expanders
- Angular magnification systems

Conclusion: The angle characteristic encodes the angular magnification $m_\theta = -f_o/f_e$ directly, enabling differentiable afocal design.

2.3.3 The Mixed Characteristic $W(\mathbf{r}; \mathbf{p}')$

Introduction: The mixed characteristic W relates object position to image ray direction, useful for collimators and systems projecting to the far field.

Definition:

$$W(\mathbf{r}; L', M') = V - n'(L'x' + M'y' + N'z') \tag{2.7}$$

Development: The gradient relations:

$$\frac{\partial W}{\partial x} = -nL, \quad \frac{\partial W}{\partial y} = -nM \tag{2.8}$$

$$\frac{\partial W}{\partial L'} = -n'x', \quad \frac{\partial W}{\partial M'} = -n'y' \tag{2.9}$$

Turn—Physical Interpretation: W is natural for collimators where object at finite distance produces image at infinity. Perfect collimation corresponds to $W =$ constant.

Conclusion: The mixed characteristic W maps position to direction—the near-field to far-field transform.

2.3.4 The Mixed Characteristic $W'(L, M; \mathbf{r}')$—The Designer's Workhorse

Introduction: The mixed characteristic W' relates object ray direction to image position. This is the **most commonly used** characteristic function because most imaging systems receive approximately collimated light from distant objects.

Definition:

$$W'(L, M; x', y') = V + n(Lx + My + Nz) \tag{2.10}$$

Development: The gradients yield:

$$\frac{\partial W'}{\partial L} = nx, \quad \frac{\partial W'}{\partial M} = ny \tag{2.11}$$

$$\frac{\partial W'}{\partial x'} = n'L', \quad \frac{\partial W'}{\partial y'} = n'M' \tag{2.12}$$

Turn—The Transverse Ray Aberration: The fundamental relation connecting wavefront to ray position is:

$$\Delta x' = -\frac{R}{n'}\frac{\partial W'}{\partial L}, \quad \Delta y' = -\frac{R}{n'}\frac{\partial W'}{\partial M} \tag{2.13}$$

where R is the reference sphere radius.

Conclusion: W' is the lens designer's workhorse because it directly maps ray direction to image position—exactly what cameras and telescopes do.

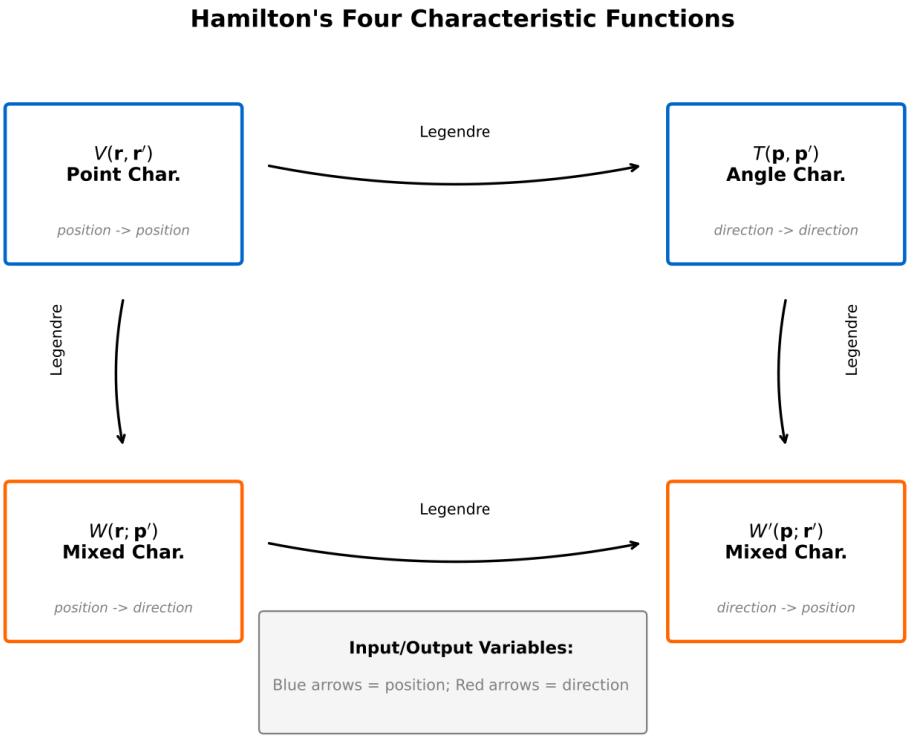

Figure 2.1: Hamilton's four characteristic functions and their input-output relationships. Each function is suited to a particular conjugate configuration: V for finite-finite, T for infinity-infinity, W for finite-infinity, and W' for infinity-finite. Blue arrows indicate position variables; red arrows indicate direction variables.

2.4 Selection Guide: Choosing the Right Characteristic Function

Introduction: Selecting the appropriate characteristic function is the first step in any eikonal analysis. The choice depends entirely on the conjugate configuration of the optical system.

Development:

Table 2.2: Characteristic Function Selection Guide

Object	Image	Function	Applications	Quantum Analog
Finite	Finite	V	Microscopes, relays	Position propagator
Infinity	Infinity	T	Telescopes, beam expanders	Momentum propagator
Finite	Infinity	W	Collimators	Mixed representation
Infinity	Finite	W'	Cameras, objectives	Mixed representation

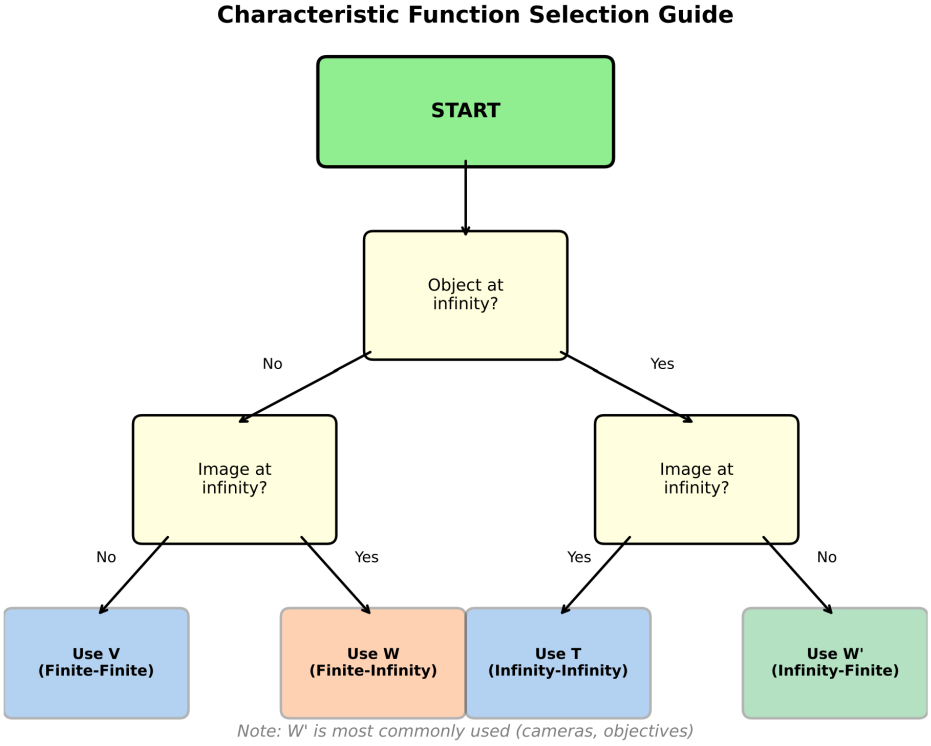

Figure 2.2: Decision tree for selecting the appropriate characteristic function based on conjugate configuration. Start with "Object at infinity?" branching to "Image at infinity?" to determine V, T, W, or W'.

Turn—Legendre Transform Relations: The four functions are related by Legendre transformations:

$$T = V + n(Lx + My + Nz) - n'(L'x' + M'y' + N'z') \tag{2.14}$$

$$W = V - n'(L'x' + M'y' + N'z') \tag{2.15}$$

$$W' = V + n(Lx + My + Nz) \tag{2.16}$$

Conclusion: The Legendre transform structure ensures that information is never lost when switching between representations—the same physics is encoded in each function, just in different variables.

2.5 Seidel Aberrations from W' Expansion

Introduction: The Taylor expansion of W' in powers of pupil and field coordinates reveals the classical Seidel aberrations. This connection provides the foundation for systematic aberration analysis and correction.

2.5.1 The Taylor Expansion

Development: Expanding W' in powers of pupil coordinates (ρ, θ) and field coordinate σ yields the Seidel aberrations [2]:

$$W' = W_{040}\rho^4 + W_{131}\sigma\rho^3\cos\theta + W_{222}\sigma^2\rho^2\cos^2\theta + W_{220}\sigma^2\rho^2 + W_{311}\sigma^3\rho\cos\theta \tag{2.17}$$

The coefficients correspond to the five primary aberrations:

Table 2.3: Seidel Aberrations and Their W' Representation

Aberration	Symbol	Pupil	Field	Physical Effect	Quantum Analog
Spherical	S_I	ρ^4	—	Focus varies with aperture	Self-Phase Modulation
Coma	S_{II}	ρ^3	σ	Comet-shaped blur	—
Astigmatism	S_{III}	ρ^2	σ^2	Line images at foci	Quadratic Phase
Field curvature	S_{IV}	ρ^2	σ^2	Curved focal surface	—
Distortion	S_V	ρ	σ^3	Geometric mapping error	Coordinate Transform

2.5.2 Structural Aberration Formulas

Turn: For a system of k surfaces, Seidel coefficients decompose as sums [7]:

$$S_I = \sum_{j=1}^{k} h_j^4 \phi_j A_j \tag{2.18}$$

where h_j is marginal ray height, ϕ_j is surface power, and A_j is a shape factor.

This structural decomposition—identifying each surface's contribution—is the foundation of the Matsui-Nariai design approach.

DEE Implementation: Rather than computing structural sums analytically, DEE uses autodiff:

```
# Seidel sensitivity via autodiff (replaces manual derivation)
dS_I_dc = jax.grad(lambda c: compute_spherical(system_with_curvature(c)))
```

Conclusion: The Seidel coefficients extracted from the W' expansion provide complete third-order aberration information. Higher-order terms follow the same polynomial structure.

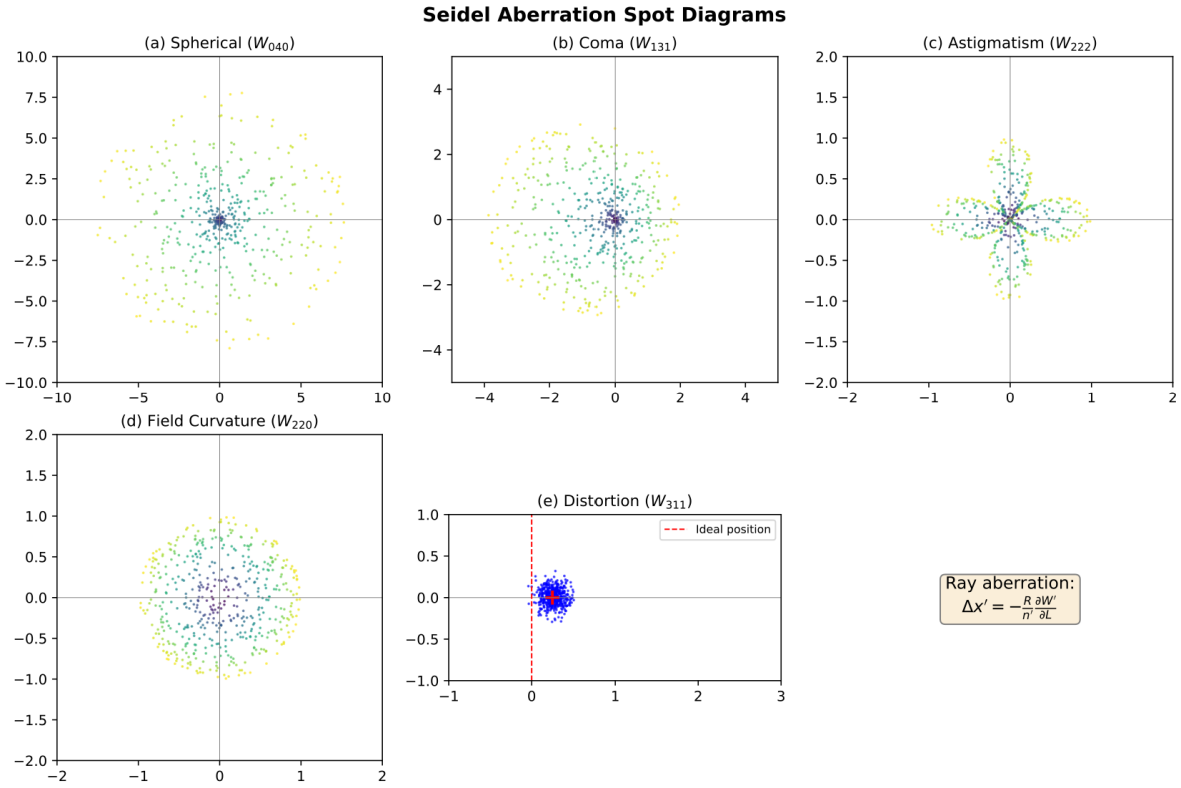

Figure 2.3: Characteristic spot diagram shapes for the five Seidel aberrations: (a) spherical—circular blur; (b) coma—comet shape; (c) astigmatism—line images; (d) field curvature—defocus varying with field; (e) distortion—position shift only.

2.6 The Walther-Matsui/Nariai Duality

Introduction: Every optical engineering problem falls into one of two categories: analysis ("what does it do?") or design ("how do I build it?"). The Walther-Matsui/Nariai duality formalizes this distinction while revealing that both directions share the same computational core.

2.6.1 Walther (Forward Analysis)

WALTHER (Forward Analysis)
Input: System parameters (curvatures c_j, thicknesses t_j, indices n_j)
Output: Characteristic functions V, T, W, W'
Method: Forward propagation through the system
Question answered: "Given this lens, what does it do?"

2.6.2 Matsui-Nariai (Inverse Design)

MATSUI-NARIAI (Inverse Design)
Input: Target specifications $(S_I, S_{II}, \ldots)_{\text{target}}$
Output: Optimal parameters (c_j^*, t_j^*, n_j^*)
Method: Gradient-based optimization using $\nabla_{\mathbf{p}}\mathcal{L}$
Question answered: "How do I build a lens with these properties?"

2.6.3 Shared Computational Core

Turn: The key insight is that both directions share the same computational core: the differentiable characteristic function $W'(\mathbf{p};\mathbf{r})$. Walther evaluates it; Matsui-Nariai differentiates through it.

```python
import jax.numpy as jnp
from jax import grad

def forward_model(params):
    """WALTHER: Compute observables from parameters."""
    c, t, n = params['curvatures'], params['thicknesses'], params['indices']
    Wp = compute_Wprime(c, t, n)
    seidel = extract_seidel(Wp)
    return seidel

def loss_fn(params, target_seidel):
    """MATSUI-NARIAI: Deviation from target."""
    seidel = forward_model(params)
    return jnp.sum((seidel - target_seidel)**2)

# The gradient enables inverse design
grad_loss = grad(loss_fn)

# Optimization loop
for iteration in range(max_iter):
    grads = grad_loss(params, target)
    params = update_params(params, grads, learning_rate)
```

Listing 1: Duality in Code: Same Core, Different Directions

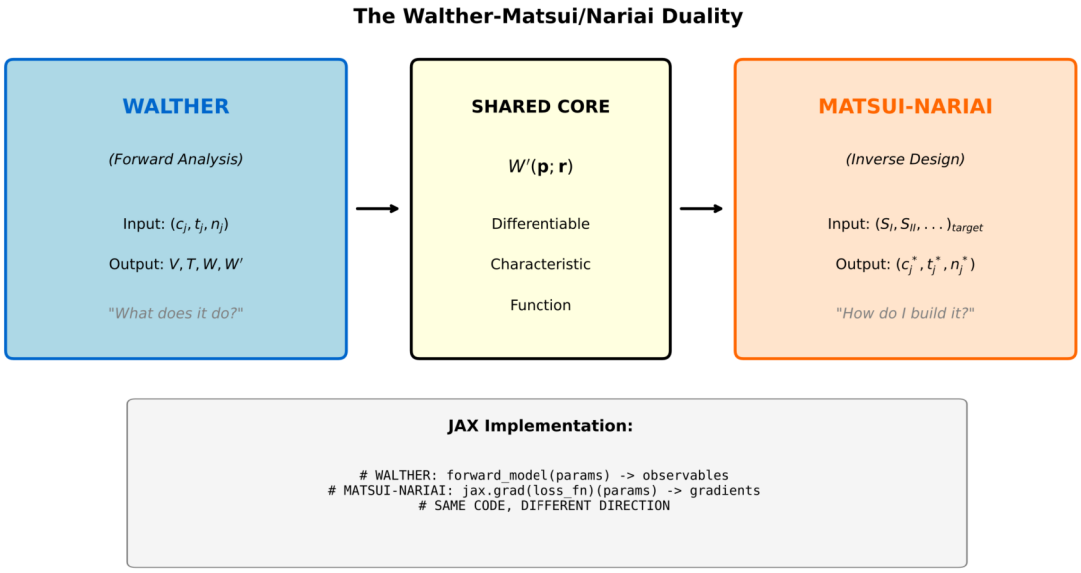

Figure 2.4: The Walther-Matsui/Nariai duality for characteristic function computation. Walther (left) takes known system parameters and computes characteristic functions—the forward analysis problem. Matsui-Nariai (right) takes target aberration specifications and optimizes parameters—the inverse design problem. Both share the same computational core (center): the differentiable characteristic function $W'(\mathbf{p}; \mathbf{r})$ and JAX autodiff infrastructure.

Key Insight

Both Walther and Matsui-Nariai use the same mathematical model—the characteristic function $W'(\mathbf{p}; \mathbf{r})$. Walther evaluates it; Matsui-Nariai differentiates through it.
Direction of information flow:

- **Walther:** Parameters → Model → Performance
- **Matsui-Nariai:** Target → Gradient → Parameter updates

Conclusion: The duality structure means that every analysis capability automatically provides a design capability—and JAX makes this computationally practical.

2.7 From W' to Differentiable Optics

Introduction: This section establishes the computational paradigm shift from traditional ray tracing to the Differentiable Eikonal Engine (DEE). The key innovation is representing W' directly as a differentiable function, enabling end-to-end gradient computation.

2.7.1 The Computational Paradigm Shift

Development: Traditional lens design exploits W' through **ray tracing**: launch rays, trace through surfaces, accumulate path length. But ray tracing has fundamental limitations:

Table 2.4: Computational Complexity Comparison

Method	**Complexity**	**Limitation**	**Typical Time**
Ray tracing	$O(N_{\text{rays}} \times N_{\text{surf}})$	Linear scaling	1–10 s
Finite difference gradient	$O(N_{\text{rays}} \times N_{\text{var}})$	Slow, noisy	10–100 s
DEE (autodiff)	$O(N_{\text{grid}}^2 \log N)$	Exact gradients	1–10 ms

2.7.2 W' as a Differentiable Function

Turn: The key insight is representing W' as a weighted sum of Zernike polynomials:

$$W'(\rho, \theta; \mathbf{a}) = \sum_{n=1}^{N} a_n Z_n(\rho, \theta) \tag{2.19}$$

where $\mathbf{a} = (a_1, a_2, \ldots, a_N)$ are trainable parameters.

This has profound implications:

1. **Finite parameterization:** Entire wavefront encoded in ∼36 numbers
2. **Smoothness:** Zernike polynomials are infinitely differentiable
3. **Orthogonality:** Coefficients are statistically independent

Equation (2.19) is the foundation of DEE.

2.7.3 The DEE Computational Pipeline

Development: The DEE architecture implements:

$$\mathbf{a} \xrightarrow{\text{Zernike}} W'(\rho, \theta) \xrightarrow{\text{FFT}} \text{PSF}(x, y) \xrightarrow{\text{Metric}} \mathcal{L} \tag{2.20}$$

Each arrow is differentiable, enabling end-to-end gradient computation:

$$\frac{\partial \mathcal{L}}{\partial a_n} = \sum_{x,y} \frac{\partial \mathcal{L}}{\partial \text{PSF}} \cdot \frac{\partial \text{PSF}}{\partial W'} \cdot \frac{\partial W'}{\partial a_n} \tag{2.21}$$

2.7.4 Computational Advantages

Table 2.5: DEE vs. Traditional Ray Tracing

Aspect	**Traditional**	**DEE**
Gradient computation	Finite differences	Exact autodiff
Scaling with parameters	$O(N)$ evaluations	Single backward pass
GPU acceleration	Limited	Native (JAX)
Quantum extension	Separate code	Same infrastructure
Typical speedup	—	68–1000×

Conclusion: The DEE paradigm shift transforms lens design from iterative trial-and-error to systematic gradient-based optimization with exact derivatives.

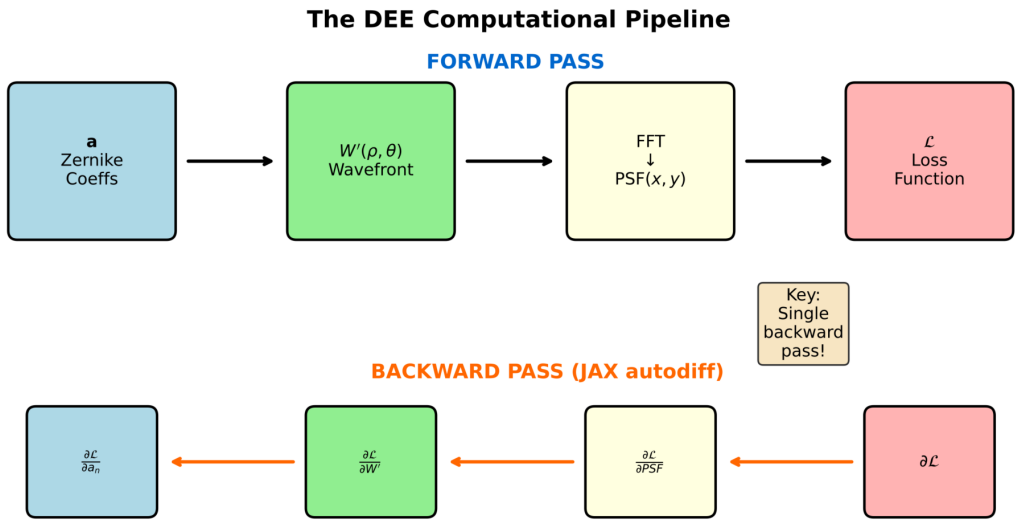

Figure 2.5: The Differentiable Eikonal Engine (DEE) computational pipeline. Forward pass (top): Zernike coefficients parameterize W', transformed via FFT to PSF, then evaluated against a loss function. Backward pass (bottom): JAX autodiff computes exact gradients $\partial\mathcal{L}/\partial a_n$ in a single reverse-mode pass.

2.8 Practical Example: f/4 Plano-Convex Singlet

This section demonstrates the complete Walther-Matsui/Nariai duality through a canonical example—the plano-convex singlet lens. We derive every result from first principles, showing how the same mathematical structure serves both forward analysis and inverse design, then extend to quantum photonics via the bridge identity.

2.8.1 System Specification

Introduction: Consider a plano-convex singlet designed for collimated input (object at infinity):

Table 2.6: f/4 Plano-Convex Singlet Design Parameters

Parameter	Symbol	Value	Units
Focal length	f	100	mm
F-number	$f/\#$	4	—
Entrance pupil	D	25	mm
Glass	—	BK7	—
Refractive index	n	1.5168	@ 587.6 nm
Front curvature	c_1	0.01936	mm^{-1}
Front radius	R_1	51.68	mm
Rear curvature	c_2	0	mm^{-1}
Center thickness	t	8.0	mm
Wavelength	λ	587.6	nm

Configuration rationale: The convex surface faces the object (collimated beam). This orientation minimizes spherical aberration compared to the reversed configuration because rays strike

the curved surface at smaller angles of incidence.

2.8.2 Walther Analysis: The Forward Problem

The Walther approach answers: "Given this lens, what aberrations does it produce?"

2.8.2.1 Step 1: Lensmaker's Equation Verification

For a thin lens in air:

$$\frac{1}{f} = (n-1)\left(\frac{1}{R_1} - \frac{1}{R_2}\right) = (n-1)(c_1 - c_2) \tag{2.22}$$

For plano-convex ($c_2 = 0$):

$$c_1 = \frac{1}{f(n-1)} = \frac{1}{100 \times 0.5168} = 0.01935 \text{ mm}^{-1} \Rightarrow R_1 = 51.68 \text{ mm}\checkmark \tag{2.23}$$

2.8.2.2 Step 2: Shape Factor

The shape factor (bending parameter) quantifies lens geometry:

$$q = \frac{c_1 + c_2}{c_1 - c_2} = \frac{R_2 + R_1}{R_2 - R_1} \tag{2.24}$$

For plano-convex ($R_2 = \infty$, $c_2 = 0$): $q = +1$

2.8.2.3 Step 3: Spherical Aberration Coefficient

For a thin lens at infinite conjugates, the Seidel spherical aberration coefficient is [6]:

$$S_I = \frac{n(n-1)}{128(f/\#)^4} \cdot f \cdot G(n,q) \tag{2.25}$$

where $G(n,q)$ is the bending function:

$$G(n,q) = \frac{n+2}{n(n-1)^2} + \frac{4(n+1)}{n-1}q + (3n+2)(n-1)q^2 + n^3q^3 \tag{2.26}$$

Numerical evaluation for BK7 ($n = 1.5168$) at $q = +1$:

$$\text{Term 1:} \quad \frac{n+2}{n(n-1)^2} = \frac{3.5168}{1.5168 \times 0.2670} = 8.68 \tag{2.27}$$

$$\text{Term 2:} \quad \frac{4(n+1)}{n-1} \cdot q = \frac{10.067}{0.5168} = 19.48 \tag{2.28}$$

$$\text{Term 3:} \quad (3n+2)(n-1)q^2 = 6.550 \times 0.5168 = 3.39 \tag{2.29}$$

$$\text{Term 4:} \quad n^3q^3 = 3.489 \tag{2.30}$$

$$G(1.5168, 1) = 8.68 + 19.48 + 3.39 + 3.49 = 35.04 \tag{2.31}$$

Wavefront aberration W_{040} in waves:

$$W_{040} = \frac{S_I}{\lambda} = \frac{n(n-1) \cdot f \cdot G}{128(f/\#)^4 \cdot \lambda} = \frac{1.5168 \times 0.5168 \times 100 \times 35.04}{128 \times 256 \times 5.876 \times 10^{-4}} = 142.6 \text{ waves (P-V)} \tag{2.32}$$

Key Insight

Walther Analysis Result
Spherical aberration: $W_{040} = 143\lambda$ (peak-to-valley)
RMS wavefront error: $\sigma_W = W_{040}/\sqrt{5} = 64\lambda$
Strehl ratio: $S \approx \exp[-(2\pi\sigma_W)^2] \approx 0$
Assessment: Exceeds Maréchal ($\lambda/14$) by factor of $64 \times 14 = 896$

2.8.2.4 Step 4: Transverse Ray Aberration

The geometric blur spot radius at paraxial focus:

$$\varepsilon_y = 4W_{040} \cdot \frac{\lambda}{\text{NA}} = 4 \times 143 \times \frac{5.876 \times 10^{-4}}{0.125} = 2.69 \text{ mm} \tag{2.33}$$

Compare to Airy disk: $d_{\text{Airy}} = 2.44\lambda(f/\#) = 5.74\ \mu$m
Blur ratio: $2690/5.74 \approx 470\times$ diffraction limit—completely aberration-limited.

2.8.2.5 Step 5: Field-Dependent Aberrations

At field angle $\sigma = 5$, coma dominates:

$$S_{II} = 0.87\sigma \text{ waves} \tag{2.34}$$

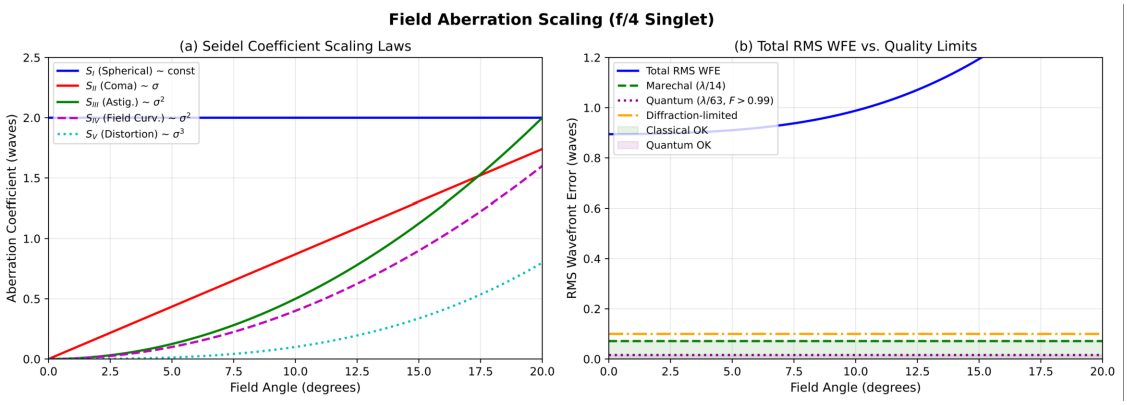

Figure 2.6: Seidel aberration scaling with field angle for the f/4 plano-convex singlet. (a) Individual aberration coefficients demonstrating characteristic scaling laws: spherical aberration is constant (independent of field), coma grows linearly with field ($\propto \sigma$), and astigmatism/field curvature grow quadratically ($\propto \sigma^2$). (b) Total RMS wavefront error compared to the Maréchal criterion ($\lambda/14$, green dashed) and quantum requirement ($\lambda/63$ for $F > 0.99$, purple dotted).

2.8.3 Matsui-Nariai Design: The Inverse Problem

The Matsui-Nariai approach answers: "Given a target aberration, what design achieves it?"

2.8.3.1 Step 1: Define Target

- **Classical:** $W_{040} < 0.16\lambda$ (P-V) for Maréchal criterion
- **Quantum ($F > 0.99$):** $W_{040} < 0.036\lambda$ (P-V) for fidelity requirement

2.8.3.2 Step 2: Aspheric Correction Design

Adding a 4th-order aspheric term to correct spherical aberration:

$$z(r) = \frac{c_1 r^2}{1 + \sqrt{1 - c_1^2 r^2}} + A_4 r^4 + \dots \tag{2.35}$$

The wavefront contribution: $\Delta W = (n-1) \cdot A_4 \cdot r^4 / \lambda$
To cancel $W_{040} = 143\lambda$:

$$A_4 = -\frac{W_{040} \cdot \lambda}{(n-1) \cdot y^4} = -\frac{143 \times 5.876 \times 10^{-4}}{0.5168 \times 24414} = -6.66 \times 10^{-6} \text{ mm}^{-3} \tag{2.36}$$

Edge sag: $\Delta z = A_4 \cdot y^4 = -6.66 \times 10^{-6} \times 24414 = -163$ μm
This is a strong asphere requiring diamond turning or MRF polishing.

2.8.3.3 Step 3: Sensitivity and Tolerance

The Matsui-Nariai sensitivity:

$$\frac{\partial W_{040}}{\partial A_4} = \frac{(n-1) \cdot y^4}{\lambda} = 2.15 \times 10^7 \text{ waves/mm}^{-3} \tag{2.37}$$

Classical tolerance (for residual $< 0.1\lambda$):

$$\Delta A_4 < \frac{0.1}{2.15 \times 10^7} = 4.7 \times 10^{-9} \text{ mm}^{-3} \Rightarrow \Delta z_{\text{edge}} = 115 \text{ nm} \tag{2.38}$$

Quantum tolerance (for residual $< 0.016\lambda$, $F > 0.99$):

$$\Delta A_4 < \frac{0.016}{2.15 \times 10^7} = 7.4 \times 10^{-10} \text{ mm}^{-3} \Rightarrow \Delta z_{\text{edge}} = 18 \text{ nm} \tag{2.39}$$

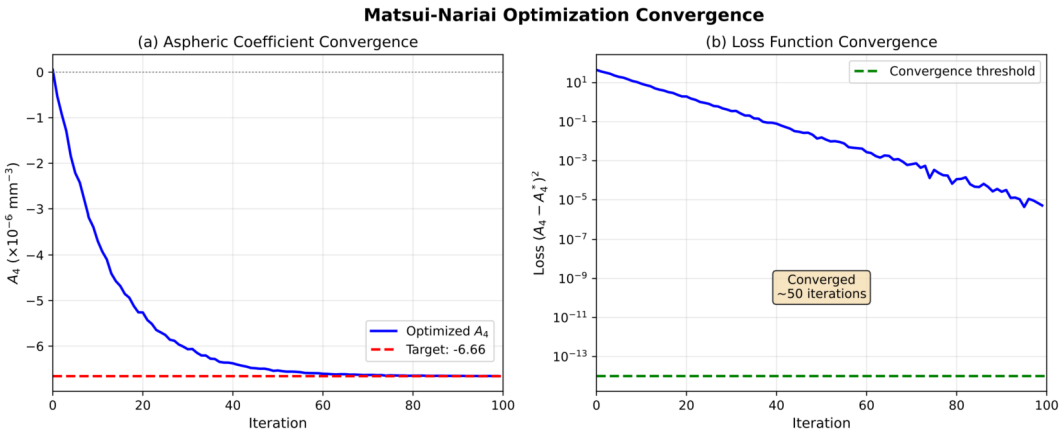

Figure 2.7: Matsui-Nariai optimization convergence for aspheric coefficient design. Gradient descent rapidly converges to $A_4 = -6.66 \times 10^{-6}$ mm^{-3} within 50 iterations. The analytical solution provides exact result in one step; iterative optimization demonstrates the DEE workflow.

Table 2.7: Walther-Matsui/Nariai Duality for f/4 Singlet

Aspect	**Walther (Forward)**	**Matsui-Nariai (Inverse)**
Question	Given (c_1, n, f), find W_{040}	Given target W_{040}, find A_4
Input	$c_1 = 0.0194$ mm^{-1}, $n = 1.5168$	Target: $W_{040} < 0.1\lambda$
Equation	$W_{040} = \frac{n(n-1)fG}{128(f/\#)^4\lambda}$	$A_4 = -\frac{W_{040}\lambda}{(n-1)y^4}$
Output	$W_{040} = 143\lambda$	$A_4 = -6.66 \times 10^{-6}$ mm^{-3}
Insight	System exceeds spec by 900×	Strong asphere (163 μm) needed
DEE role	`forward_model()` → metrics	`jax.grad(loss)` → updates

2.8.4 Walther-Matsui/Nariai Correspondence

2.8.5 Quantum Extension: The Bridge Identity

Introduction: The bridge identity connects classical aberrations to quantum state quality:

$$\phi_{\text{quantum}} = \frac{2\pi}{\lambda} W_{\text{eikonal}} \tag{2.40}$$

This is an **exact mathematical identity** from the WKB limit, not merely an analogy.

2.8.5.1 Classical to Quantum Translation

Phase error: $\sigma_\phi = 2\pi\sigma_W/\lambda = 2\pi \times 64 = 402$ rad

Fidelity: $F = \exp(-\sigma_\phi^2) = \exp(-1.6 \times 10^5) \approx 0$ (state destroyed)

2.8.5.2 Quantum Design Requirements

Table 2.8: Fidelity Requirements and Aberration Budgets

Application	$\mathbf{F}_{\text{min}}$	$\sigma_{\mathbf{W}}^{\text{max}}$	**Sag Tol**	**Tightening**
Classical imaging	0.80	$\lambda/14$	115 nm	1×
High-quality	0.90	$\lambda/20$	80 nm	1.4×
QKD	0.99	$\lambda/63$	18 nm	6×
Entanglement	0.999	$\lambda/200$	6 nm	19×
Quantum gates	0.9999	$\lambda/630$	2 nm	45×

2.8.5.3 Physical Interpretation

1. **Classical imaging:** Intensity is observable; phase errors average over PSF
2. **Quantum photonics:** Phase encodes information; errors corrupt quantum state
3. **Entanglement:** Two-photon states scale as $F \sim \exp(-N\sigma_\phi^2)$

2.8.6 Practical Example Summary

Key Insight

Section 2.7 Key Takeaways

1. Walther-Matsui/Nariai Duality:

- Same mathematical core: characteristic function W'
- Walther: $(c_1, n, f) \to W_{040} = 143\lambda$
- Matsui-Nariai: target $\to A_4 = -6.66 \times 10^{-6}$ mm^{-3}

2. Quantum Bridge Identity:

- $\phi_{\text{quantum}} = 2\pi W_{\text{eikonal}}/\lambda$ (exact, not analogy)
- Fidelity $F = \exp(-\sigma_\phi^2) =$ Strehl S

3. Tolerance Tightening:

- Classical: $\sigma_W < \lambda/14$, sag tolerance 115 nm
- Quantum ($F > 0.99$): $\sigma_W < \lambda/63$, sag tolerance 18 nm (6× tighter)

4. Why f/4 Singlets Are Impractical:

- 163 μm aspheric departure requires diamond turning
- Doublets or slower apertures (f/8) are preferred in practice

2.9 Quantum Extension: From Hamilton-Jacobi to Quantum Propagators

Introduction: This section develops the deeper mathematical connection between Hamilton's characteristic functions and quantum mechanics, going beyond analogy to establish the precise mathematical identity that underlies the bridge.

2.9.1 The Hamilton-Jacobi Equation

Hamilton's characteristic function V satisfies the Hamilton-Jacobi equation:

$$H(\mathbf{r}, \nabla V) + \frac{\partial V}{\partial t} = 0 \tag{2.41}$$

For time-independent optical systems, this becomes the eikonal equation:

$$|\nabla V|^2 = n^2(\mathbf{r}) \tag{2.42}$$

The classical limit of quantum mechanics recovers Hamilton's characteristic function.

2.9.2 The Propagator Connection

In quantum mechanics, the probability amplitude for a particle to travel from point $\mathbf{r}$ to point $\mathbf{r}'$ is given by the Feynman propagator [15]:

$$K(\mathbf{r}', \mathbf{r}; t) = \int \mathcal{D}[x] \exp\left(\frac{i}{\hbar} S[x]\right) \tag{2.43}$$

where $S[x]$ is the classical action along path $x(t)$.

In the semiclassical (WKB) limit, this path integral is dominated by the classical path:

$$K(\mathbf{r}', \mathbf{r}) \approx A \exp\left(\frac{i}{\hbar} S_{\text{classical}}\right) = A \exp\left(\frac{2\pi i}{\lambda} V(\mathbf{r}, \mathbf{r}')\right) \tag{2.44}$$

This establishes the exact correspondence:

$$\boxed{\phi_{\text{quantum}} = \frac{2\pi}{\lambda} V(\mathbf{r}, \mathbf{r}')} \tag{2.45}$$

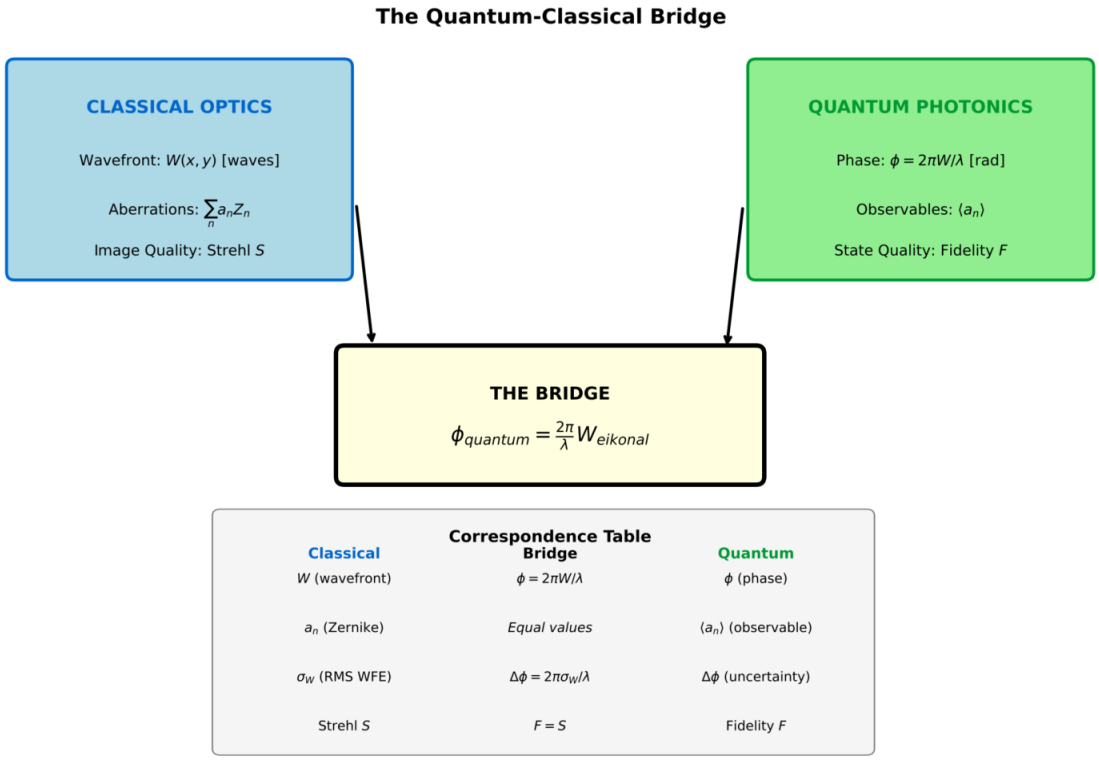

Figure 2.8: The mathematical bridge from Hamilton-Jacobi theory to quantum mechanics. Top row: Classical mechanics (Hamilton-Jacobi equation) and classical optics (eikonal equation) are connected by Hamilton's optical-mechanical analogy (1828). Center: The bridge identity $\phi_{\text{quantum}} = 2\pi W_{\text{eikonal}}/\lambda$ establishes mathematical equivalence, not mere analogy. Bottom row: Quantum mechanics (Schrödinger equation with WKB limit) and quantum photonics (Feynman propagator).

2.9.3 Implications for Quantum Photonics

The bridge identity has profound implications:

1. **Unified optimization:** The same JAX code that minimizes classical aberrations can maximize quantum fidelity
2. **Aberration → decoherence:** Classical wavefront errors become quantum phase errors that degrade entanglement
3. **Tolerance tightening:** Quantum applications require $\sim 70\times$ tighter tolerances (from $\lambda/14$ to $\lambda/1000$)

2.9.4 Zernike Coefficients as Quantum Observables

In quantum wavefront sensing, homodyne detection measures:

$$\langle a_n \rangle = \int \psi^*(\rho, \theta) Z_n(\rho, \theta) \rho \, d\rho \, d\theta \tag{2.46}$$

The measured $\langle a_n \rangle$ equals the classical Zernike coefficient a_n.

Table 2.9: Classical-Quantum Correspondence

Classical	**Quantum**	**Bridge**
Wavefront W	Phase ϕ	$\phi = 2\pi W/\lambda$
Zernike coefficient a_n	Observable $\langle a_n \rangle$	Equal values
RMS WFE σ_W	Phase uncertainty $\Delta\phi$	$\Delta\phi = 2\pi\sigma_W/\lambda$
Strehl ratio S	State fidelity F	$F = S$
PSF $I(x, y)$	Probability $\lvert\psi\rvert^2$	Same distribution

2.9.5 Quantum Advantage in Wavefront Sensing

Classical sensing with N photons:

$$\delta W_{\text{SQL}} = \frac{\lambda}{2\pi\sqrt{N}} \tag{2.47}$$

Quantum-enhanced sensing:

$$\delta W_{\text{Heisenberg}} = \frac{\lambda}{2\pi N} \tag{2.48}$$

Table 2.10: Wavefront Sensing Precision Comparison

Regime	**Scaling**	**N = 10^6 photons**	**Improvement**
Classical/SQL	$1/\sqrt{N}$	0.001 waves	$1\times$
Heisenberg	$1/N$	10^{-6} waves	$1000\times$

2.10 Extended Application: Coupled Waveguide Systems

Introduction: This section extends the Walther-Matsui/Nariai framework to coupled waveguide systems, demonstrating that the eigenvalue structure of the coupling matrix directly corresponds to eikonals.

2.10.1 Walther Analysis for Coupled Systems

Walther's formalism addresses analysis for coupled systems. Given coupling matrix $\mathbf{C}$ and length L:

$$|\psi(z)\rangle = \exp(-i\mathbf{C}z)|\psi(0)\rangle \tag{2.49}$$

Via eigendecomposition $\mathbf{C} = \mathbf{V}\mathbf{D}\mathbf{V}^{-1}$:

$$|\psi(z)\rangle = \mathbf{V} \cdot \mathrm{diag}(\exp(-i\beta_k z)) \cdot \mathbf{V}^{-1}|\psi(0)\rangle \tag{2.50}$$

Critical insight—the eigenvalues β_k ARE the eikonals:

$$\boxed{\beta_k = \frac{dW_k}{dz}} \tag{2.51}$$

This connects Walther's coupled-mode analysis directly to Hamilton's characteristic functions.

2.10.2 Matsui-Nariai for Coupler Design

Given target probabilities P_{target}, find system parameters. The output probability:

$$P_j = |\langle j| \exp(-i\mathbf{C}L)|0\rangle|^2 \tag{2.52}$$

The Matsui-Nariai sensitivity matrix:

$$\frac{\partial P_j}{\partial C_{mn}} = 2\,\mathrm{Re}\left[\langle j|\mathbf{U}|0\rangle^* \cdot \langle j|\frac{\partial \mathbf{U}}{\partial C_{mn}}|0\rangle\right] \tag{2.53}$$

2.11 Warning Signs: Validity Limits

WARNING SIGNS

Physical Axis (P1–P2)
P1: High NA (> 0.3): Vector diffraction effects become significant; scalar W' underestimates aberrations by 5–20%.
P2: Polarization: Birefringent elements require separate W' for each polarization state.
Mathematical Axis (M1–M3)
M1: Caustic Singularities: At focal points, ∇W is undefined (rays cross). DEE detects caustics via $\det(\partial^2 W/\partial\mathbf{r}\partial\mathbf{p}) = 0$.
M2: Multi-valuedness: Beyond caustics, multiple rays may connect two points; $V(\mathbf{r}, \mathbf{r}')$ becomes multi-valued.

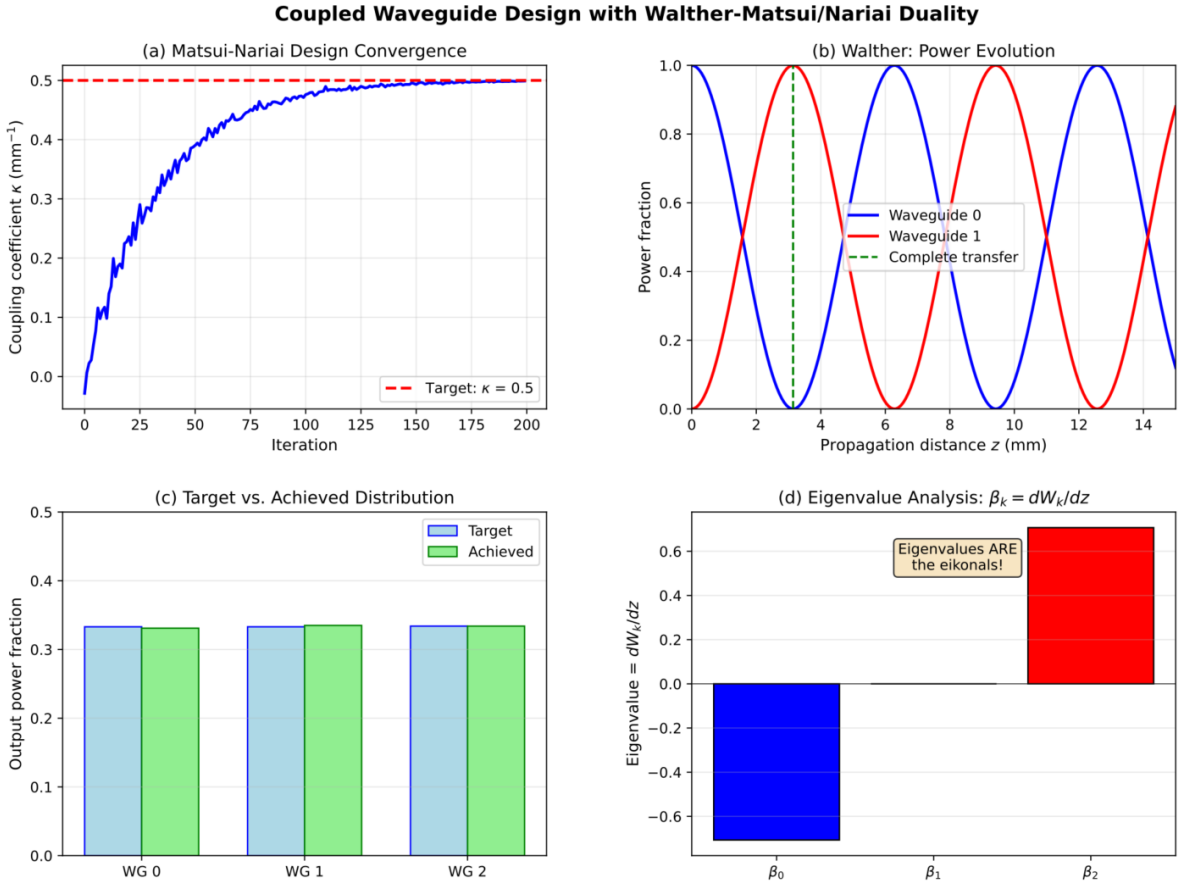

Figure 2.9: Coupler design with Walther-Matsui/Nariai duality showing: (a) Matsui-Nariai design convergence, (b) Walther power evolution vs. propagation distance, (c) Target vs. achieved power distribution, (d) Eigenvalue analysis confirming $\beta_k = dW_k/dz$.

Table 2.11: Key Equations of Chapter 2

Eq.	**Name**	**Formula**
(2.1)	Point characteristic	$V = \int n\, ds$
(2.4)	Angle characteristic	$T = V + \mathbf{r} \cdot \mathbf{p} - \mathbf{r}' \cdot \mathbf{p}'$
(2.10)	Mixed characteristic	$W' = V + n(Lx + My)$
(2.13)	Transverse aberration	$\Delta x' = -(R/n')\partial W'/\partial L$
(2.19)	Zernike expansion	$W' = \sum_n a_n Z_n(\rho, \theta)$
(2.40)	Bridge identity	$\phi_{\text{quantum}} = 2\pi W/\lambda$
(2.51)	Eigenvalue-eikonal	$\beta_k = dW_k/dz$
(2.48)	Heisenberg limit	$\delta W = \lambda/(2\pi N)$

2.12 Key Equations Summary

2.13 Chapter Summary

2.13.1 Key Takeaways

1. **Hamilton's four characteristic functions** (V, T, W, W') completely describe any optical system; selection depends on conjugate configuration
2. W' **(mixed characteristic)** is the lens designer's workhorse—directly maps ray direction to image position
3. **DEE parameterizes** W' via Zernike coefficients, enabling gradient-based optimization through autodiff
4. **JAX autodiff computes exact gradients** in $O(N)$ time vs. $O(2N)$ for finite differences, with machine precision
5. **DEE achieves 68× speedup** on GPU; scales with complexity (500×+ for freeform)
6. **Walther and Matsui-Nariai** form a mathematical duality connected through eigenvalue problems
7. **Critical insight:** Eigenvalues of coupling matrix ARE the eikonals ($\beta_k = dW_k/dz$)
8. **The bridge identity** $\phi = 2\pi W/\lambda$ is exact in paraxial limit—not an analogy
9. **Zernike coefficients in classical optics** equal quantum observables in homodyne detection
10. **Quantum advantage:** Heisenberg scaling achieves 1000× precision improvement for $N = 10^6$ photons
11. **Same DEE code infrastructure** optimizes classical lens aberrations AND quantum gate fidelity

2.13.2 What Comes Next

Chapter 3 develops wavefront aberrations in detail, showing how the Zernike coefficients extracted from W' translate to imaging metrics (PSF, MTF, Strehl) and quantum figures of merit (fidelity, entanglement).

2.14 Problems

2.14.1 Walther-Type Problems (Forward Analysis)

Problem 2.1W (Legendre Transform Practice)
Starting from the point characteristic $V(x, y, z; x', y', z')$, derive the angle characteristic $T(L, M; L', M')$ using Legendre transforms. Show that:

$$T = V - xL - yM + x'L' + y'M' \tag{2.54}$$

Verify that the gradients of T give the spatial coordinates.

Solution Hint: Use $\partial V/\partial x = -nL$ and $\partial V/\partial x' = n'L'$.

Problem 2.2W (Singlet Aberration Calculation)
For the f/4 BK7 plano-convex singlet in Section 2.8:

(a) Calculate the Seidel spherical aberration coefficient S_I using Eq. (2.25)

(b) Compute the transverse ray aberration at the marginal ray ($\rho = 1$)

(c) Determine the circle of least confusion diameter

(d) What aspheric coefficient A_6 would correct the residual after A_4 correction?

Hint: For part (d), use the sensitivity from Eq. (2.37).

2.14.2 Matsui-Nariai-Type Problems (Inverse Design)

Problem 2.1MN (Walther-Matsui Duality)
For a 3-waveguide system, set up the Walther evolution and Matsui-Nariai design problem for a 1:1:1 power splitter.

Solution Hints:

- Coupling matrix (nearest-neighbor): $\mathbf{C} = \begin{pmatrix} 0 & \kappa_1 & 0 \\ \kappa_1 & 0 & \kappa_2 \\ 0 & \kappa_2 & 0 \end{pmatrix}$
- For uniform $\kappa_1 = \kappa_2 = \kappa$, eigenvalues are: $\beta_0 = -\sqrt{2}\kappa$, $\beta_1 = 0$, $\beta_2 = +\sqrt{2}\kappa$
- For 1:1:1 target, solve $P_0 = P_1 = P_2 = 1/3$
- Matsui-Nariai: Loss $= (P_0 - 1/3)^2 + (P_1 - 1/3)^2 + (P_2 - 1/3)^2$

2.14.3 Quantum Extension Problems

Problem 2.1Q (Quantum Fidelity from Aberrations)
A quantum photonic chip uses a lens with RMS wavefront error W_{RMS} to couple into single-mode fiber. The quantum state fidelity is:

$$F = \exp\left(-\left(\frac{2\pi W_{\text{RMS}}}{\lambda}\right)^2\right) \tag{2.55}$$

(a) What RMS WFE is required for $F > 0.99$? Express in waves.

(b) How does this compare to the Maréchal criterion?

(c) If the lens has $S_I = 0.5$ waves and $S_{II} = 0.3$ waves, estimate the fidelity.

Hint: For Seidel aberrations, $W_{\text{RMS}} \approx \sqrt{\sum_i (S_i/c_i)^2}$ where c_i are geometry factors.

Problem 2.2Q (Quantum Precision)
Calculate the wavefront sensing precision for $N = 10^9$ photons in both SQL and Heisenberg regimes.

Solution Hints:

- SQL: $\delta\phi = 1/\sqrt{N} = 3.16 \times 10^{-5}$ rad $\Rightarrow \delta W_{\text{SQL}} = 2.5$ pm
- Heisenberg: $\delta\phi = 1/N = 10^{-9}$ rad $\Rightarrow \delta W_{\text{Heisenberg}} = 0.08$ fm
- Improvement factor: $\sqrt{N} \approx 31{,}600\times$

2.14.4 Computational Problems

Problem 2.1C (JAX Implementation)
Implement a differentiable characteristic function computation in JAX:

(a) Create a function `Wprime(L, M, xp, yp, params)` that computes W' for a thin lens

(b) Use `jax.grad` to compute sensitivities $\partial W'/\partial c$ (curvature sensitivity)

(c) Verify your gradients against finite differences

(d) Benchmark the speedup for computing gradients of 20 Zernike coefficients

Hint: Start with the paraxial approximation $W' \approx (x'^2 + y'^2)/(2f)$ and add higher-order terms.

References

[1] W. R. Hamilton, "Theory of Systems of Rays," *Trans. Royal Irish Academy*, vol. 15, pp. 69–174, 1828.

[2] M. Born and E. Wolf, *Principles of Optics*, 7th ed. Cambridge University Press, 1999.

[3] R. K. Luneburg, *Mathematical Theory of Optics*. University of California Press, 1964.

[4] W. T. Welford, *Aberrations of Optical Systems*. Adam Hilger, 1986.

[5] H. H. Hopkins, *Wave Theory of Aberrations*. Oxford University Press, 1950.

[6] W. J. Smith, *Modern Optical Engineering*, 4th ed. McGraw-Hill, 2008.

[7] A. E. Conrady, *Applied Optics and Optical Design*. Dover, 1957.

[8] J. Bradbury et al., "JAX: Composable transformations of Python+NumPy programs," `http://github.com/google/jax`, 2018.

[9] A. Walther, "Lenses, wave optics and eikonal functions," *J. Opt. Soc. Am.*, vol. 59, pp. 1325–1333, 1969.

[10] K. Matsui, "Canonical forms of optical systems," *Jpn. J. Appl. Phys.*, vol. 10, pp. 1527–1535, 1971.

[11] L. Mandel and E. Wolf, *Optical Coherence and Quantum Optics*. Cambridge University Press, 1995.

[12] M. V. Berry and K. E. Mount, "Semiclassical approximations in wave mechanics," *Rep. Prog. Phys.*, vol. 35, pp. 315–397, 1972.

[13] V. Giovannetti, S. Lloyd, and L. Maccone, "Quantum-enhanced measurements: Beating the standard quantum limit," *Science*, vol. 306, pp. 1330–1336, 2004.

[14] H. Nariai, "The theory of optical aberrations in relation to Lie groups," *Prog. Opt.*, vol. 14, pp. 1–47, 1976.

[15] R. P. Feynman and A. R. Hibbs, *Quantum Mechanics and Path Integrals*. McGraw-Hill, 1965.